inclusion increases in skeletal muscle tissue during normal postnatal development of mice [17]. However, we found that α-dystrobrevin Δvr3, which should be the fetal isoform in mouse, is expressed exclusively in adult human muscle, and the relative amount of α-dystrobrevin +vr3 is higher in human fetal, than in adult, cardiac muscle [17]. These results suggest a different, or possibly an opposite, mode of regulation of vr3 alternative splicing between human and mouse. Since this portion, as described below, corresponds to one of syntrophin binding sites, these results might imply a functional difference of α-dystrobrevin between mice and human. Recently, Bohm *et al.* extensively analyzed the differences in α-dystrobrevin splicing between human and mouse [18]. They also showed the opposite mode of vr3 splicing regulation between human and mouse (exon 12 and 13 by their numbering method). In addition, they found another novel exon just upstream of the vr3. The exon is alternatively spliced in human but not in mice, and suggested to contain another syntrophin binding motif, although the transcripts containing this exon are less expressed in skeletal muscle.

Figure 1. Alternative splicing of human α-dystrobrevin. Exons represented as thick boxes are translated segments and thin boxes indicate untranslated segments. The exon numbering is based on [10], which is different from that proposed by [18]. Introns and downstream flanking regions are represented by horizontal lines. Gray boxes represent the alternatively spliced exons: variable regions 1 (vr1), 2 (vr2), and 3 (vr3). The different isoforms of protein are represented below. The identifiable domains are boxed: EF, EF hand region; ZZ, zinc-binding domain; CC, coiled-coil domain; Y, unique tyrosine kinase substrate domain. Suggested syntrophin binding sites (SBS) and dystrophin binding site (DBS) are indicated. This figure is a modified version of an illustration in [17].

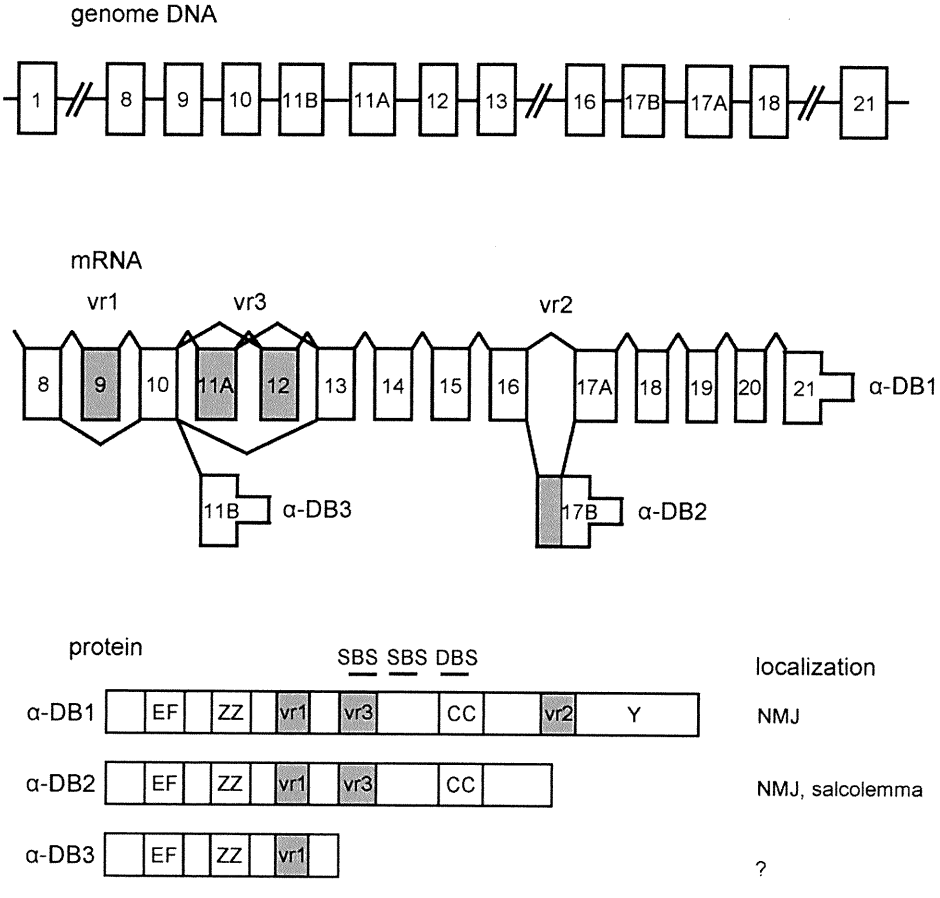

3. Structure of Dystrobrevin Protein and Localization in Striated Muscle

α-Dystrobrevin is comprised of four major domains, two EF-hand motifs that potentially bind calcium, a ZZ-domain, an α-helical coiled-coil domain containing a dystrophin binding site, and a tyrosine kinase substrate domain (Figure 1) [7]. α-Dystrobrevin 1, α-dystrobrevin 2 and α-dystrobrevin 3 bind to the sarcoglycan complex via the *N*-terminal region [8]. α-Dystrobrevin 1 and α-dystrobrevin 2 bind dystrophin through the highly conserved coiled-coil domain [2,7]. α-Dystrobrevin 1 and α-dystrobrevin 2 have syntrophin binding sites at the upstream of the coiled-coil domain [19].

α-Dystrobrevin 1, which has a unique *C*-terminal tyrosine kinase substrate domain [1,4], is localized in the sarcolemma and is abundant at the neuromuscular junction (NMJ), especially in the crest of the junctional folds [11,14,15,20]. α-Dystrobrevin 2 is localized around the entire circumference of the sarcolemmal membrane including the NMJ, and concentrated in the troughs of the folds [11]. α-Dystrobrevin 2 co-localizes with only dystrophin at the NMJ, while α-dystrobrevin 1 co-localizes with both dystrophin as well as utrophin which shares structural and functional similarities with dystrophin [11]. α-Dystrobrevin 3, which lacks both syntrophin and dystrophin binding sites, is capable of binding to the sarcoglycan complex via the *N*-terminal region [8]. α-Dystrobrevin 3 has been suggested to be localized in the cytoplasm [21].

4. The Role of Dystrobrevin for Structural Integrity of Muscle—Interaction with Cytoskeletal Binding Partners

α-Dystrobrevin is a component of DGC, which is indispensable for the structural integrity of muscle. As mentioned above, it directly associates with dystrophin at its coiled-coil domain and with sarcoglycan complex in its *N*-terminal half. As is the case with dystrophin, α-dystrobrevin may also function as a structural scaffold linking the DGC to the intracellular cytoskeleton. By using the yeast two-hybrid and co-immunoprecipitation analysis, several groups identified additional α-dystrobrevin-binding proteins: syncoilin, β-synemin, and dysbindin [22–24] (Figure 2). Syncoilin and β-synemin are both intermediate filament (IF) proteins. The IFs play a structural role by forming an important part of the cell cytoskeleton and providing mechanical stability to the cells [25]. In muscle cells, the IFs encircle the Z-lines of each integral myofibril, thereby connecting all adjacent myofibrils and linking the Z-lines of the peripheral layer of cellular myofibrils to the sarcolemma [26].

Syncoilin is highly expressed in striated muscle, and co-localizes with α-dystrobrevin at the NMJ and sarcolemma. Syncoilin interacts with α-dystrobrevin via vr3 and its flanking region [22]. Syncoilin also binds to desmin, a muscle-specific intermediate filament protein, and has been thought to organize desmin filaments to the Z-line [27]. The α-dystrobrevin/syncoilin interaction provides a further physical linkage between the DGC and the cytoskeleton, in addition to the well-characterized linkage between dystrophin and actin. Interestingly, syncoilin-null mice show a reduced force-generating capacity, suggesting that the link with syncoilin may be important for force transduction during contraction, although the DGC is still intact without syncoilin [28]. In addition, the increased syncoilin immunolabeling was reported in the sarcolemma of immature regenerating fibers in patients with Duchene muscular dystrophy [29] and mouse models of muscle disease [22]. This suggests that

syncoilin and its binding partner, α-dystrobrevin +vr3, may be required for muscle regeneration in response to injury.

Figure 2. Schematic illustration of the dystrophin-glycoprotein complex network in muscle. α-Dystrobrevin (α-DB) forms a core part of the DGC with dystrophin, syntrophin, α-dystroglycan (α-DG), β-dystroglycan (β-DG), sarcoglycan complex (SGC), and sarcospan (SPN). Proteins involved in structural integrity and signaling are highlighted in purple and red, respectively.

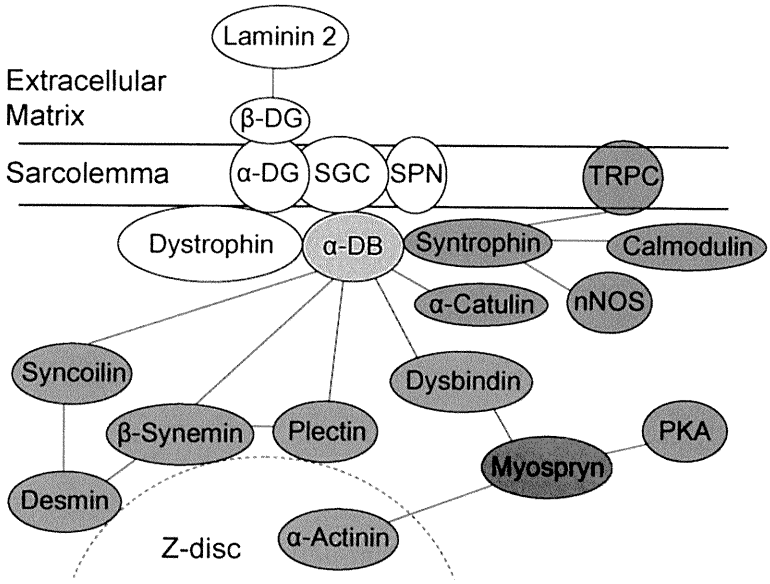

β-Synemin is a large, heteropolymeric IF protein that forms IFs with other major IF proteins, such as desmin [23]. β-Synemin interacts and co-localizes with α-dystrobrevin at the NMJ and myotendinous junction (MTJ) [23,30]. The α-dystrobrevin/β-synemin interaction provides another connection between the IF networks and the DGC. Furthermore, β-synemin interacts with plectin, a linker protein of IFs to Z-discs [31]. Interestingly, plectin is also suggested to interact directly with α-dystrobrevin. Taken together, these interactions between α-dystrobrevin and IF proteins would stabilize the sarcolemma and protect it against contraction-imposed stress by tethering IFs to the DGC at the sarcolemma (Figure 2).

Dysbindin is a ubiquitously expressed coiled-coil-containing protein, although the expression in muscle is relatively low [24]. In skeletal muscle, dysbindin is located at the sarcolemma. Dysbindin binds to α-dystrobrevin through coiled-coil domains and interact with myospryn [24,32]. Lastly, myospryn is a muscle-specific protein, localized to the sarcolemmal region of skeletal muscle. Myospryn is suggested to function as a docking platform for additional structural proteins and signaling molecules, such as α-actinin 2 and protein kinase A, respectively [33,34].

5. The Role of Dystrobrevin in Signaling—Interaction with Syntrophin

α-Dystrobrevin 1 and α-dystrobrevin 2 bind directly with syntrophin, which is a modular adaptor protein thought to be involved in signaling [35–38] (Figure 2). Skeletal muscle contains several isoforms—α-, β1-, β2-, and γ2-syntrophin—encoded by different genes [38–42]. α-Syntrophin is the

major isoform in skeletal and cardiac muscles [36,38,41], being expressed in the sarcolemma and NMJ [14,20]. β1-Syntrophin also localizes at the sarcolemma and NMJ, whereas β2- and γ2-syntrophin are largely confined to the NMJ. With regard to the syntrophin binding site on Torpedo 87K protein, a homologue of human α-dystrobrevin 1, Dwyer *et al.* mapped the α-syntrophin binding site to a region analogous to exons 12–13 of human α-dystrobrevin [37], and Ahn *et al.* reported a β1-syntrophin binding site in a region corresponding to exons 13–14 of human α-dystrobrevin [36]. From yeast two-hybrid study, Newey *et al.* identified another binding site situated within the vr3 region in mouse, and suggested that α-dystrobrevin contains two independent syntrophin binding sites in tandem [43]. Recently, we directly confirmed that α-syntrophin interacts with α-dystrobrevin via the vr3 domain in human muscle and revealed dramatic decrease in binding between α-syntrophin and α-dystrobrevin mutant in vr3 [17]. α-Syntrophin knockout mice exhibit marked hypertrophy during muscle regeneration and deranged NMJ accompanied by impaired ability to exercise, suggesting a role of α-syntrophin in the regulation of muscle volume and formation of highly organized NMJ [44,45].

Syntrophin has the potential to co-ordinate the assembly of several important proteins such as neuronal nitric oxide synthase (nNOS) [46], stress-activated protein kinase-3 [47], Grb2 [48], and calmodulin [49,50] to the DGC. nNOS generates NO from L-arginine in many different cells. nNOS at the sarcolemma regulates local blood flow in contracting skeletal muscle in part by antagonizing sympathetic vasoconstriction [51]. The expression of nNOS is decreased in many muscular dystrophies, resulting in decreased vasodilation [52]. Consistent with nNOS being associated with α-syntrophin in muscle, α-syntrophin knockout mice lack sarcolemmal nNOS [53]. It is also reported that normalized production of NO protects dystrophin-deficient *mdx* muscle from degeneration [54]. Recently, transient receptor potential channels (TRPCs) were also found to associate with α-syntrophin [55]. These channels anchored to the DGC are suggested to form a signaling complex that modulates cation entry and regulates calcium homeostasis in skeletal muscles [56]. Calcium homeostasis and calcium-dependent signaling pathways play an important role in regulating muscle contractility, metabolism, and gene expression [57]. Thus, these signaling pathways via α-dystrobrevin/syntrophin may have a significant impact on muscle function.

Very recently, α-catulin, a catenin/vinculin-related molecule, was identified as a binding partner of α-dystrobrevin 1 [58]. α-Catulin, which co-localizes with α-dystrobrevin at nerve bundles and blood vessels, is thought to regulate α_{1D}-adrenergic receptor signal transduction. It was shown that α-catulin interact with α-dystrobrevin 1 at its *C*-terminal domain. Since α-catulin is ubiquitously expressed, including in skeletal muscle [59], the interaction between α-dystrobrevin and α-catulin may be involved in some forms of receptor-mediated signaling in skeletal muscle.

6. Dystrobrevin in Muscle Disease

Despite the evidence that abnormalities of the DGC components cause various muscular dystrophies, so far no mutation in α-dystrobrevin has been reported in muscular dystrophy patients. However, a missense mutation was found in a four-generation Japanese family with left ventricular non-compaction (LVNC) [60], a cardiomyopathy, often associated with neuromuscular disorders [61]. LVNC is characterized by a pattern of prominent trabecular meshwork and deep inter-trabecular recesses, and is thought to be caused by arrest of normal endomyocardial morphogenesis [62].

Histological analysis showed that the level of α-dystrobrevin is greatly reduced at the sarcolemma of patients with DMD and SD-LGMD, suggesting that dystrophin and sarcoglycan are required for anchorage of α-dystrobrevin at the sarcolemma [21]. On the other hand, Jones *et al.* analyzed the expression of α-dystrobrevin by immunohistochemistry in biopsies from 162 patients with myopathies of unknown etiology with normal staining for dystrophin and other dystrophin-associated proteins [14]. Among the patients, deficiency of α-dystrobrevin was found in 16 patients, while no mutation was identified in the coding region of the α-dystrobrevin gene. Although there was a significant variety in severity and age of onset, all patients presented with congenital-onset hypotonia and weakness, indicating a new disease entity caused by α-dystrobrevin deficiency.

In addition, mice lacking α-dystrobrevin exhibit skeletal and cardiac myopathies, defects of NMJ maturation, and abnormal myotendinous junctions [9,63,64]. At NMJs in α-dystrobrevin knockout mice, the distribution of acetylcholine receptor (AChR) becomes granular in appearance with ragged edges. Myotube cultures from α-dystrobrevin knockout mice forms normal AChR clusters; however, these clusters quickly disappear into micro-aggregates, suggesting that α-dystrobrevin is not required for initial formation of the postsynaptic apparatus at the NMJ, but indispensable for its maturation and stabilization. Despite the presence of a structurally intact DGC in the sarcolemma, these mice show a striking displacement of nNOS from the sarcolemma and impaired NO-mediated signaling [9]. Moreover, the biochemical association between dystrophin and β-dystroglycan is impaired in α-dystrobrevin knockout mice, suggesting a role for α-dystrobrevin in stabilizing the DGC [65].

Furthermore, we revealed mis-regulated alternative splicing of α-dystrobrevin in muscle from myotonic dystrophy type 1 (DM1) patients [17]. DM1 is proposed as a "spliceopathy", *i.e.*, a *trans*-effect on the alternative splicing of many RNAs, leading to inappropriate expression of aberrantly spliced products, such as Cl channel, ryanodine receptor and dystrophin [66–69]. α-Dystrobrevin mRNA including vr3 is increased in both skeletal and cardiac muscle of DM1 patients. Interestingly, the splicing abnormality is correlated with the muscular disability of DM1. The aberrantly spliced α-dystrobrevin isoform has an increased binding capacity for α-syntrophin, thereby recruiting excess α-syntrophin to the sarcolemma in DM1 muscle.

7. Concluding Remarks

A number of proteins that comprise the link between striated muscle Z-disc and peripheral structures, such as the costamere, have been discovered. Recent studies suggest that this protein network acts as a structural and signaling center for striated muscle to ensure coordinated contractile activity. The importance of the network to normal muscle function has emerged from investigations into the causes of muscular dystrophies and cardiomyopathies. One of the key players in the network is α-dystrobrevin that mediates signaling and structural function of the DGC. Although functional differences among the various splicing variants and detailed roles of their counterparts still remain unknown, future studies will shed much more light on the importance of α-dystrobrevin in striated muscle and implications for muscular dystrophy.

Acknowledgements

This work was supported by Intramural Research Grant (20B-13) for Neurological and Psychiatric Disorders of NCNP, Research Grants for Intractable Disease from the Ministry of Health Labour and Welfare, and grants-in-aid for Scientific Research from the Japan Society for the Promotion of Science to M.P.T., and by postdoctoral fellowships from the Cell Science Research Foundation and the Uehara Memorial Foundation to M.N.

References

1. Wagner, K.R.; Cohen, J.B.; Huganir, R.L. The 87K postsynaptic membrane protein from Torpedo is a protein-tyrosine kinase substrate homologous to dystrophin. *Neuron* **1993**, *10*, 511–522.
2. Blake, D.J.; Tinsley, J.M.; Davies, K.E.; Knight, A.E.; Winder, S.J.; Kendrick-Jones, J. Coiled-coil regions in the carboxy-terminal domains of dystrophin and related proteins: Potentials for protein-protein interactions. *Trends Biochem. Sci.* **1995**, *20*, 133–135.
3. Sadoulet-Puccio, H.M.; Khurana, T.S.; Cohen, J.B.; Kunkel, L.M. Cloning and characterization of the human homologue of a dystrophin related phosphoprotein found at the Torpedo electric organ post-synaptic membrane. *Hum. Mol. Genet.* **1996**, *5*, 489–496.
4. Blake, D.J.; Nawrotzki, R.; Peters, M.F.; Froehner, S.C.; Davies, K.E. Isoform diversity of dystrobrevin, the murine 87-kDa postsynaptic protein. *J. Biol. Chem.* **1996**, *271*, 7802–7810.
5. Lapidos, K.A.; Kakkar, R.; McNally, E.M. The dystrophin glycoprotein complex: Signaling strength and integrity for the sarcolemma. *Circ. Res.* **2004**, *94*, 1023–1031.
6. Ozawa, E.; Noguchi, S.; Mizuno, Y.; Hagiwara, Y.; Yoshida, M. From dystrophinopathy to sarcoglycanopathy: Evolution of a concept of muscular dystrophy. *Muscle Nerve* **1998**, *21*, 421–438.
7. Sadoulet-Puccio, H.M.; Rajala, M.; Kunkel, L.M. Dystrobrevin and dystrophin: An interaction through coiled-coil motifs. *Proc. Natl. Acad. Sci. USA* **1997**, *94*, 12413–12418.
8. Yoshida, M.; Hama, H.; Ishikawa-Sakurai, M.; Imamura, M.; Mizuno, Y.; Araishi, K.; Wakabayashi-Takai, E.; Noguchi, S.; Sasaoka, T.; Ozawa, E. Biochemical evidence for association of dystrobrevin with the sarcoglycan-sarcospan complex as a basis for understanding sarcoglycanopathy. *Hum. Mol. Genet.* **2000**, *9*, 1033–1040.
9. Grady, R.M.; Grange, R.W.; Lau, K.S.; Maimone, M.M.; Nichol, M.C.; Stull, J.T.; Sanes, J.R. Role for alpha-dystrobrevin in the pathogenesis of dystrophin-dependent muscular dystrophies. *Nat. Cell Biol.* **1999**, *1*, 215–220.
10. Sadoulet-Puccio, H.M.; Feener, C.A.; Schaid, D.J.; Thibodeau, S.N.; Michels, V.V.; Kunkel, L.M. The genomic organization of human dystrobrevin. *Neurogenetics* **1997**, *1*, 37–42.
11. Peters, M.F.; Sadoulet-Puccio, H.M.; Grady, M.R.; Kramarcy, N.R.; Kunkel, L.M.; Sanes, J.R.; Sealock, R.; Froehner, S.C. Differential membrane localization and intermolecular associations of alpha-dystrobrevin isoforms in skeletal muscle. *J. Cell Biol.* **1998**, *142*, 1269–1278.
12. Peters, M.F.; O'Brien, K.F.; Sadoulet-Puccio, H.M.; Kunkel, L.M.; Adams, M.E.; Froehner, S.C. beta-dystrobrevin, a new member of the dystrophin family. Identification, cloning, and protein associations. *J. Biol. Chem.* **1997**, *272*, 31561–31569.

13. Enigk, R.E.; Maimone, M.M. Differential expression and developmental regulation of a novel alpha-dystrobrevin isoform in muscle. *Gene* **1999**, *238*, 479–488.
14. Jones, K.J.; Compton, A.G.; Yang, N.; Mills, M.A.; Peters, M.F.; Mowat, D.; Kunkel, L.M.; Froehner, S.C.; North, K.N. Deficiency of the syntrophins and alpha-dystrobrevin in patients with inherited myopathy. *Neuromuscul. Disord.* **2003**, *13*, 456–467.
15. Nawrotzki, R.; Loh, N.Y.; Ruegg, M.A.; Davies, K.E.; Blake, D.J. Characterisation of alpha-dystrobrevin in muscle. *J. Cell Sci.* **1998**, *111*, 2595–2605.
16. Holzfeind, P.J.; Ambrose, H.J.; Newey, S.E.; Nawrotzki, R.A.; Blake, D.J.; Davies, K.E. Tissue-selective expression of alpha-dystrobrevin is determined by multiple promoters. *J. Biol. Chem.* **1999**, *274*, 6250–6258.
17. Nakamori, M.; Kimura, T.; Kubota, T.; Matsumura, T.; Sumi, H.; Fujimura, H.; Takahashi, M.P.; Sakoda, S. Aberrantly spliced alpha-dystrobrevin alters alpha-syntrophin binding in myotonic dystrophy type 1. *Neurology* **2008**, *70*, 677–685.
18. Bohm, S.V.; Constantinou, P.; Tan, S.; Jin, H.; Roberts, R.G. Profound human/mouse differences in alpha-dystrobrevin isoforms: A novel syntrophin-binding site and promoter missing in mouse and rat. *BMC Biol.* **2009**, *7*, 85.
19. Froehner, S.C.; Adams, M.E.; Peters, M.F.; Gee, S.H. Syntrophins: Modular adapter proteins at the neuromuscular junction and the sarcolemma. *Soc. Gen. Physiol. Ser.* **1997**, *52*, 197–207.
20. Compton, A.G.; Cooper, S.T.; Hill, P.M.; Yang, N.; Froehner, S.C.; North, K.N. The syntrophin-dystrobrevin subcomplex in human neuromuscular disorders. *J. Neuropathol. Exp. Neurol.* **2005**, *64*, 350–361.
21. Metzinger, L.; Blake, D.J.; Squier, M.V.; Anderson, L.V.; Deconinck, A.E.; Nawrotzki, R.; Hilton-Jones, D.; Davies, K.E. Dystrobrevin deficiency at the sarcolemma of patients with muscular dystrophy. *Hum. Mol. Genet.* **1997**, *6*, 1185–1191.
22. Newey, S.E.; Howman, E.V.; Ponting, C.P.; Benson, M.A.; Nawrotzki, R.; Loh, N.Y.; Davies, K.E.; Blake, D.J. Syncoilin, a novel member of the intermediate filament superfamily that interacts with alpha-dystrobrevin in skeletal muscle. *J. Biol. Chem.* **2001**, *276*, 6645–6655.
23. Mizuno, Y.; Thompson, T.G.; Guyon, J.R.; Lidov, H.G.; Brosius, M.; Imamura, M.; Ozawa, E.; Watkins, S.C.; Kunkel, L.M. Desmuslin, an intermediate filament protein that interacts with alpha -dystrobrevin and desmin. *Proc. Natl. Acad. Sci. USA* **2001**, *98*, 6156–6161.
24. Benson, M.A.; Newey, S.E.; Martin-Rendon, E.; Hawkes, R.; Blake, D.J. Dysbindin, a novel coiled-coil-containing protein that interacts with the dystrobrevins in muscle and brain. *J. Biol. Chem.* **2001**, *276*, 24232–24241.
25. Lazarides, E. Intermediate filaments as mechanical integrators of cellular space. *Nature* **1980**, *283*, 249–256.
26. Robson, R.M.; Huiatt, T.W.; Bellin, R.M. Muscle intermediate filament proteins. *Methods Cell Biol.* **2004**, *78*, 519–553.
27. Poon, E.; Howman, E.V.; Newey, S.E.; Davies, K.E. Association of syncoilin and desmin: linking intermediate filament proteins to the dystrophin-associated protein complex. *J. Biol. Chem.* **2002**, *277*, 3433–3439.

28. Zhang, J.; Bang, M.L.; Gokhin, D.S.; Lu, Y.; Cui, L.; Li, X.; Gu, Y.; Dalton, N.D.; Scimia, M.C.; Peterson, K.L.; Lieber, R.L.; Chen, J. Syncoilin is required for generating maximum isometric stress in skeletal muscle but dispensable for muscle cytoarchitecture. *Am. J. Physiol. Cell Physiol.* **2008**, *294*, C1175–C1182.
29. Brown, S.C.; Torelli, S.; Ugo, I.; de Biasia, F.; Howman, E.V.; Poon, E.; Britton, J.; Davies, K.E.; Muntoni, F. Syncoilin upregulation in muscle of patients with neuromuscular disease. *Muscle Nerve* **2005**, *32*, 715–725.
30. Mizuno, Y.; Guyon, J.R.; Watkins, S.C.; Mizushima, K.; Sasaoka, T.; Imamura, M.; Kunkel, L.M.; Okamoto, K. Beta-synemin localizes to regions of high stress in human skeletal myofibers. *Muscle Nerve* **2004,** 30, 337–346.
31. Hijikata, T.; Nakamura, A.; Isokawa, K.; Imamura, M.; Yuasa, K.; Ishikawa, R.; Kohama, K.; Takeda, S.; Yorifuji, H. Plectin 1 links intermediate filaments to costameric sarcolemma through beta-synemin, alpha-dystrobrevin and actin. *J. Cell Sci.* **2008**, *121*, 2062–2074.
32. Benson, M.A.; Tinsley, C.L.; Blake, D.J. Myospryn is a novel binding partner for dysbindin in muscle. *J. Biol. Chem.* **2004**, *279*, 10450–10458.
33. Durham, J.T.; Brand, O.M.; Arnold, M.; Reynolds, J.G.; Muthukumar, L.; Weiler, H.; Richardson, J.A.; Naya, F.J. Myospryn is a direct transcriptional target for MEF2A that encodes a striated muscle, alpha-actinin-interacting, costamere-localized protein. *J. Biol. Chem.* **2006**, *281*, 6841–6849.
34. Sarparanta, J. Biology of myospryn: What's known? *J. Muscle Res. Cell Motil.* **2008**, *29*, 177–180.
35. Butler, M.H.; Douville, K.; Murnane, A.A.; Kramarcy, N.R.; Cohen, J.B.; Sealock, R.; Froehner, S.C. Association of the Mr 58,000 postsynaptic protein of electric tissue with Torpedo dystrophin and the Mr 87,000 postsynaptic protein. *J. Biol. Chem.* **1992**, *267*, 6213–6218.
36. Ahn, A.H.; Kunkel, L.M. Syntrophin binds to an alternatively spliced exon of dystrophin. *J. Cell Biol.* **1995**, *128*, 363–371.
37. Dwyer, T.M.; Froehner, S.C. Direct binding of Torpedo syntrophin to dystrophin and the 87 kDa dystrophin homologue. *FEBS Lett.* **1995**, *375*, 91–94.
38. Ahn, A.H.; Freener, C.A.; Gussoni, E.; Yoshida, M.; Ozawa, E.; Kunkel, L.M. The three human syntrophin genes are expressed in diverse tissues, have distinct chromosomal locations, and each bind to dystrophin and its relatives. *J. Biol. Chem.* **1996**, *271*, 2724–2730.
39. Adams, M.E.; Butler, M.H.; Dwyer, T.M.; Peters, M.F.; Murnane, A.A.; Froehner, S.C. Two forms of mouse syntrophin, a 58 kd dystrophin-associated protein, differ in primary structure and tissue distribution. *Neuron* **1993**, 531–540.
40. Yang, B.; Ibraghimov-Beskrovnaya, O.; Moomaw, C.R.; Slaughter, C.A.; Campbell, K.P. Heterogeneity of the 59-kDa dystrophin-associated protein revealed by cDNA cloning and expression. *J. Biol. Chem.* **1994**, *269*, 6040–6044.
41. Peters, M.F.; Adams, M.E.; Froehner, S.C. Differential association of syntrophin pairs with the dystrophin complex. *J. Cell Biol.* **1997**, *138*, 81–93.
42. Piluso, G.; Mirabella, M.; Ricci, E.; Belsito, A.; Abbondanza, C.; Servidei, S.; Puca, A.A.; Tonali, P.; Puca, G.A.; Nigro, V. Gamma1- and gamma2-syntrophins, two novel dystrophin-binding proteins localized in neuronal cells. *J. Biol. Chem.* **2000**, *275*, 15851–15860.

43. Newey, S.E.; Benson, M.A.; Ponting, C.P.; Davies, K.E.; Blake, D.J. Alternative splicing of dystrobrevin regulates the stoichiometry of syntrophin binding to the dystrophin protein complex. *Curr. Biol.* **2000**, *10*, 1295–1298.
44. Adams, M.E.; Kramarcy, N.; Krall, S.P.; Rossi, S.G.; Rotundo, R.L.; Sealock, R.; Froehner, S.C. Absence of alpha-syntrophin leads to structurally aberrant neuromuscular synapses deficient in utrophin. *J. Cell Biol.* **2000**, *150*, 1385–1398.
45. Hosaka, Y.; Yokota, T.; Miyagoe-Suzuki, Y.; Yuasa, K.; Imamura, M.; Matsuda, R.; Ikemoto, T.; Kameya, S.; Takeda, S. Alpha1-syntrophin-deficient skeletal muscle exhibits hypertrophy and aberrant formation of neuromuscular junctions during regeneration. *J. Cell Biol.* **2002**, *158*, 1097–107.
46. Brenman, J.E.; Chao, D.S.; Gee, S.H.; McGee, A.W.; Craven, S.E.; Santillano, D.R.; Wu, Z.; Huang, F.; Xia, H.; Peters, M.F.; Froehner, S.C.; Bredt, D.S. Interaction of nitric oxide synthase with the postsynaptic density protein PSD-95 and alpha1-syntrophin mediated by PDZ domains. *Cell* **1996**, *84*, 757–767.
47. Hasegawa, M.; Cuenda, A.; Spillantini, M.G.; Thomas, G.M.; Buee-Scherrer, V.; Cohen, P.; Goedert, M. Stress-activated protein kinase-3 interacts with the PDZ domain of alpha1-syntrophin. A mechanism for specific substrate recognition. *J. Biol. Chem.* **1999**, *274*, 12626–12631.
48. Oak, S.A.; Russo, K.; Petrucci, T.C.; Jarrett, H.W. Mouse alpha1-syntrophin binding to Grb2: Further evidence of a role for syntrophin in cell signaling. *Biochemistry* **2001**, *40*, 11270–11278.
49. Madhavan, R.; Massom, L.R.; Jarrett, H.W. Calmodulin specifically binds three proteins of the dystrophin-glycoprotein complex. *Biochem. Biophys. Res. Commun.* **1992**, *185*, 753–759.
50. Iwata, Y.; Pan, Y.; Yoshida, T.; Hanada, H.; Shigekawa, M. Alpha1-syntrophin has distinct binding sites for actin and calmodulin. *FEBS Lett.* **1998**, *423*, 173–177.
51. Thomas, G.D.; Sander, M.; Lau, K.S.; Huang, P.L.; Stull, J.T.; Victor, R.G. Impaired metabolic modulation of alpha-adrenergic vasoconstriction in dystrophin-deficient skeletal muscle. *Proc. Natl. Acad. Sci. USA* **1998**, *95*, 15090–15095.
52. Dalkilic, I.; Kunkel, L.M. Muscular dystrophies: Genes to pathogenesis. *Curr. Opin. Genet. Dev.* **2003**, *13*, 231–238.
53. Kameya, S.; Miyagoe, Y.; Nonaka, I.; Ikemoto, T.; Endo, M.; Hanaoka, K.; Nabeshima, Y.; Takeda, S. alpha1-syntrophin gene disruption results in the absence of neuronal-type nitric-oxide synthase at the sarcolemma but does not induce muscle degeneration. *J. Biol. Chem.* **1999**, *274*, 2193–2200.
54. Wehling, M.; Spencer, M.J.; Tidball, J.G. A nitric oxide synthase transgene ameliorates muscular dystrophy in mdx mice. *J. Cell Biol.* **2001**, *155*, 123–131.
55. Vandebrouck, A.; Sabourin, J.; Rivet, J.; Balghi, H.; Sebille, S.; Kitzis, A.; Raymond, G.; Cognard, C.; Bourmeyster, N.; Constantin, B. Regulation of capacitative calcium entries by alpha1-syntrophin: association of TRPC1 with dystrophin complex and the PDZ domain of alpha1-syntrophin. *FASEB J.* **2007**, *21*, 608–617.
56. Sabourin, J.; Lamiche, C.; Vandebrouck, A.; Magaud, C.; Rivet, J.; Cognard, C.; Bourmeyster, N.; Constantin, B. Regulation of TRPC1 and TRPC4 cation channels requires an alpha1-syntrophin-dependent complex in skeletal mouse myotubes. *J. Biol. Chem.* **2009**, *284*, 36248–36261.

57. Treves, S.; Anderson, A.A.; Ducreux, S.; Divet, A.; Bleunven, C.; Grasso, C.; Paesante, S.; Zorzato, F. Ryanodine receptor 1 mutations, dysregulation of calcium homeostasis and neuromuscular disorders. *Neuromuscul. Disord.* **2005**, *15*, 577–587.
58. Lyssand, J.S.; Whiting, J.L.; Lee, K.S.; Kastl, R.; Wacker, J.L.; Bruchas, M.R.; Miyatake, M.; Langeberg, L.K.; Chavkin, C.; Scott, J.D.; Gardner, R.G.; Adams, M.E.; Hague, C. α-Dystrobrevin-1 recruits α-catulin to the α1D-adrenergic receptor/dystrophin-associated protein complex signalosome. *Proc. Natl. Acad. Sci. USA* **2010**, *107*, 21854–21859.
59. Janssens, B.; Staes, K.; van Roy, F. Human alpha-catulin, a novel alpha-catenin-like molecule with conserved genomic structure, but deviating alternative splicing. *Biochim. Biophys. Acta* **1999**, *1447*, 341–347.
60. Ichida, F.; Tsubata, S.; Bowles, K.R.; Haneda, N.; Uese, K.; Miyawaki, T.; Dreyer, W.J.; Messina, J.; Li, H.; Bowles, N.E.; Towbin, J.A. Novel gene mutations in patients with left ventricular noncompaction or Barth syndrome. *Circulation* **2001**, *103*, 1256–1263.
61. Stollberger, C.; Winkler-Dworak, M.; Blazek, G.; Finsterer, J. Left ventricular hypertrabeculation/ noncompaction with and without neuromuscular disorders. *Int. J. Cardiol.* **2004**, *97*, 89–92.
62. Ichida, F. Left ventricular noncompaction. *Circ. J.* **2009**, *73*, 19–26.
63. Grady, R.M.; Zhou, H.; Cunningham, J.M.; Henry, M.D.; Campbell, K.P.; Sanes, J.R. Maturation and maintenance of the neuromuscular synapse: Genetic evidence for roles of the dystrophin—glycoprotein complex. *Neuron* **2000**, *25*, 279–293.
64. Grady, R.M.; Akaaboune, M.; Cohen, A.L.; Maimone, M.M.; Lichtman, J.W.; Sanes, J.R. Tyrosine-phosphorylated and nonphosphorylated isoforms of alpha-dystrobrevin: Roles in skeletal muscle and its neuromuscular and myotendinous junctions. *J. Cell Biol.* **2003**, *160*, 741–752.
65. Bunnell, T.M.; Jaeger, M.A.; Fitzsimons, D.P.; Prins, K.W.; Ervasti, J.M. Destabilization of the dystrophin-glycoprotein complex without functional deficits in alpha-dystrobrevin null muscle. *PLoS One* **2008**, *3*, e2604.
66. Mankodi, A.; Takahashi, M.P.; Jiang, H.; Beck, C.L.; Bowers, W.J.; Moxley, R.T.; Cannon, S.C.; Thornton, C.A. Expanded CUG repeats trigger aberrant splicing of ClC-1 chloride channel pre-mRNA and hyperexcitability of skeletal muscle in myotonic dystrophy. *Mol. Cell* **2002**, *10*, 35–44.
67. Kimura, T.; Nakamori, M.; Lueck, J.D.; Pouliquin, P.; Aoike, F.; Fujimura, H.; Dirksen, R.T.; Takahashi, M.P.; Dulhunty, A.F.; Sakoda, S. Altered mRNA splicing of the skeletal muscle ryanodine receptor and sarcoplasmic/endoplasmic reticulum Ca^{2+}-ATPase in myotonic dystrophy type 1. *Hum. Mol. Genet.* **2005**, *14*, 2189–2200.
68. Osborne, R.J.; Thornton, C.A. RNA-dominant diseases. *Hum. Mol. Genet.* **2006**, *15*, R162–R169.
69. Nakamori, M.; Kimura, T.; Fujimura, H.; Takahashi, M.P.; Sakoda, S. Altered mRNA splicing of dystrophin in type 1 myotonic dystrophy. *Muscle Nerve* **2007**, *36*, 251–257.

RESEARCH ARTICLE

Human Mutation

OFFICIAL JOURNAL
HGVS
HUMAN GENOME VARIATION SOCIETY
www.hgvs.org

A Mutation in a Rare Type of Intron in a Sodium-Channel Gene Results in Aberrant Splicing and Causes Myotonia

Tomoya Kubota,[1†] Xavier Roca,[2†] Takashi Kimura,[3] Yosuke Kokunai,[1] Ichizo Nishino,[4] Saburo Sakoda,[1‡] Adrian R. Krainer,[2] and Masanori P. Takahashi[1*]

[1]*Department of Neurology, Osaka University Graduate School of Medicine, Suita, Osaka, Japan;* [2]*Cold Spring Harbor Laboratory, Cold Spring Harbor, New York;* [3]*Division of Neurology, Department of Internal Medicine, Hyogo College of Medicine, Nishinomiya, Hyogo, Japan;* [4]*Department of Neuromuscular Research, National Institute of Neuroscience, National Center of Neurology and Psychiatry, Kodaira, Tokyo, Japan*

Communicated by Mario Tosi

Received 18 November 2010; accepted revised manuscript 25 February 2011.
Published online 15 March 2011 in Wiley Online Library (www.wiley.com/humanmutation). DOI 10.1002/humu.21501

ABSTRACT: Many mutations in the skeletal-muscle sodium-channel gene *SCN4A* have been associated with myotonia and/or periodic paralysis, but so far all of these mutations are located in exons. We found a patient with myotonia caused by a deletion/insertion located in intron 21 of *SCN4A*, which is an AT-AC type II intron. This is a rare class of introns that, despite having AT-AC boundaries, are spliced by the major or U2-type spliceosome. The patient's skeletal muscle expressed aberrantly spliced *SCN4A* mRNA isoforms generated by activation of cryptic splice sites. In addition, genetic suppression experiments using an *SCN4A* minigene showed that the mutant 5′ splice site has impaired binding to the U1 and U6 snRNPs, which are the cognate factors for recognition of U2-type 5′ splice sites. One of the aberrantly spliced isoforms encodes a channel with a 35-amino acid insertion in the cytoplasmic loop between domains III and IV of Nav1.4. The mutant channel exhibited a marked disruption of fast inactivation, and a simulation in silico showed that the channel defect is consistent with the patient's myotonic symptoms. This is the first report of a disease-associated mutation in an AT-AC type II intron, and also the first intronic mutation in a voltage-gated ion channel gene showing a gain-of-function defect.
Hum Mutat 32:773–782, 2011. © 2011 Wiley-Liss, Inc.

KEY WORDS: skeletal muscle; myotonia; splicing; gain of function; simulation; channelopathy

Introduction

Genetic defects in voltage-gated sodium channel (Nav) genes are responsible for several hereditary diseases [George, 2005]. Physiological studies of the mutant channels have revealed two types of functional defects, characterized by loss or reduction of conductivity (loss of function) or by altered gating (gain of function). Mutations in the skeletal-muscle sodium-channel gene *SCN4A* (MIM# 603967) are usually associated with myotonia and/or periodic paralysis and in a rare case with fatigable weakness (congenital myasthenia), and this type of disorder is inherited in an autosomal-dominant fashion [Cannon, 2006; Tsujino et al., 2003]. All of the identified mutations in *SCN4A* are located in the coding regions (exons), and the mutant Nav1.4 channels show gain-of-function defects, such as disruption of fast inactivation and/or enhancement of activation [Cannon, 2006]. To our knowledge, no mutations in *SCN4A* have been reported in noncoding regions (introns). Although disease-associated mutations located in noncoding regions have been identified in other voltage-gated ion channel genes, they generally show loss-of-function defects [Colding-Jorgensen, 2005; Dutzler et al., 2002; Ruan et al., 2009; Zimmer and Surber, 2008].

Pre-mRNA splicing relies on conserved, yet highly diverse sequence elements at both ends of introns, termed splice sites [Brow, 2002]. The vast majority of introns are bounded by GT-AG dinucleotides, and are usually recognized and spliced by the major or U2-type spliceosome, which comprises the U1, U2, U4, U5, and U6 small nuclear ribonucleoprotein particles (snRNPs) [Sheth et al., 2006]. In contrast, AT-AC introns are rare (0.34%) and usually spliced by the minor or U12-type spliceosome, comprising U11, U12, U4atac, U5, and U6atac snRNPs [Burge et al., 1998; Patel and Steitz, 2003; Sheth et al., 2006]. AT-AC introns occur frequently in voltage-gated ion channel genes, such as intron 2 and intron 21 in *SCN4A* [Wu and Krainer, 1996, 1997, 1999]. However, whereas intron 2 is spliced by the minor spliceosome, intron 21 is spliced by the major or U2-type spliceosome. Thus, intron 2 is classified as AT-AC type I, and intron 21 as AT-AC type II [Wu and Krainer, 1996, 1997]. Analogously, a small subset of GT-AG introns spliced by the minor spliceosome, further demonstrating that the terminal intronic dinucleotides do not hold enough information to determine their mechanism of recognition [Burge et al., 1998; Dietrich et al., 1997; Wu and Krainer, 1997]. A recent genomic study estimated only 15 AT-AC type II introns in the human genome (out of $\sim 2 \times 10^5$ introns), confirming that these introns are extremely rare [Sheth et al., 2006]. Furthermore, 10 out of the 15 AT-AC type II introns are found in

Additional Supporting Information may be found in the online version of this article.

[†]Contributed equally and should be considered joint first authors.

[‡]Present address: Department of Neurology, Toneyama Hospital, National Hospital Organization, Toyonaka, Osaka, Japan 5608552.

*Correspondence to: Masanori P. Takahashi, Department of Neurology, Osaka University Graduate School of Medicine, D4, 2-2, Yamadaoaka, Suita, Osaka 565-0871, Japan. E-mail: mtakahas@neurol.med.osaka-u.ac.jp

Contract grant sponsors: Intramural Research Grant for Neurological and Psychiatric Disorders of National Center of Neurology and Psychiatry 20B-13; Research Grants for Intractable Disease from the Ministry of Health Labour and Welfare; Grants-in-aid for Scientific Research from the JSPS; The Nakatomi Foundation (to M.P.T.); The National Institutes of Health; Contract grant number: GM42699 (to X.R. and A.R.K.).

members of the *Nav* channel gene family, and clearly have a common evolutionary origin [Wu and Krainer, 1997, 1999].

We found a patient with prominent myotonia caused by a deletion/insertion located in intron 21 of one of the *SCN4A* alleles. This is the first disease-associated mutation in the very rare class of AT-AC type II introns. The patient's skeletal muscle expressed aberrantly spliced *SCN4A* mRNA isoforms by activation of cryptic splice sites, and we observed the same aberrant splicing patterns when we tested mutant *SCN4A* minigenes. We further showed that the aberrantly spliced isoform encodes a channel with a 35-amino-acid insertion in the cytoplasmic loop, and this mutant channel exhibited a marked disruption of fast inactivation. In addition, we showed, using in silico simulation, that the defect of the channel is consistent with the patient's myotonic symptoms. This is the first case of a gain-of-function intronic mutation in a voltage-gated ion-channel gene.

Materials and Methods

Patient

The patient was a 35-year-old Japanese male with hypertrophic musculature (Fig. 1A). His family was not consanguineous and had no history of neuromuscular diseases. Due to myotonia, he had difficulties in opening his eyes and presented narrow palpebral fissures, which were exacerbated by repetitive contractions (eyelid paramyotonia). His distal extremities were atrophic and he had grade 2 muscle strength in the arms and grade 4 in the legs. Scoliosis was present and articular contractures were noted in shoulders, elbows, and wrists. Percussion myotonia in *abductor pollicis brevis* and *rectus abdominus* muscles and grip myotonia were present (Supp. Movies S1 and S2). Myotonia was exacerbated by cold exposure but not by intake of fruits. He also had difficulty in breathing, which probably was caused by myotonia of respiratory muscles. Administration of mexiletine alleviated his myotonic symptoms, including the difficulty in breathing. More detailed medical history is given in the Supporting Information.

Clinical Electrophysiological Examination

Clinical electrophysiological examinations were performed using Neuropack MEB 2216 (Nihon Kohden, Tokyo, Japan). In brief, needle electromyography was performed with *biceps brachii*, *extensor digitrum communis*, and *tibialis anterior* muscles using a concentric recording needle with a sampling frequency of 10 Hz–10 kHz. The compound muscle action potentials (CMAPs) of *abductor digiti minimi* were evoked by supramaximal stimulation of the ulnar nerve for 0.2 msec. The repeated short exercise test was performed as previously reported [Fournier et al., 2004, 2006].

Pathological Examination

After obtaining informed consent, a muscle specimen was extracted from the *gluteus maximus* muscle during surgery for a femur neck fracture. The specimens were snap frozen in isopentane cooled with dry ice, and stored at −80°C. Sections were stained with a battery of histochemical methods, including hematoxylin-eosin (H&E), ATPase (pH 10.2, pH 4.6, and pH 4.2) and acetylcholinesterase (AChE).

DNA Sequencing

We obtained informed consent from patients and family members enrolled in the study, using protocols approved by the

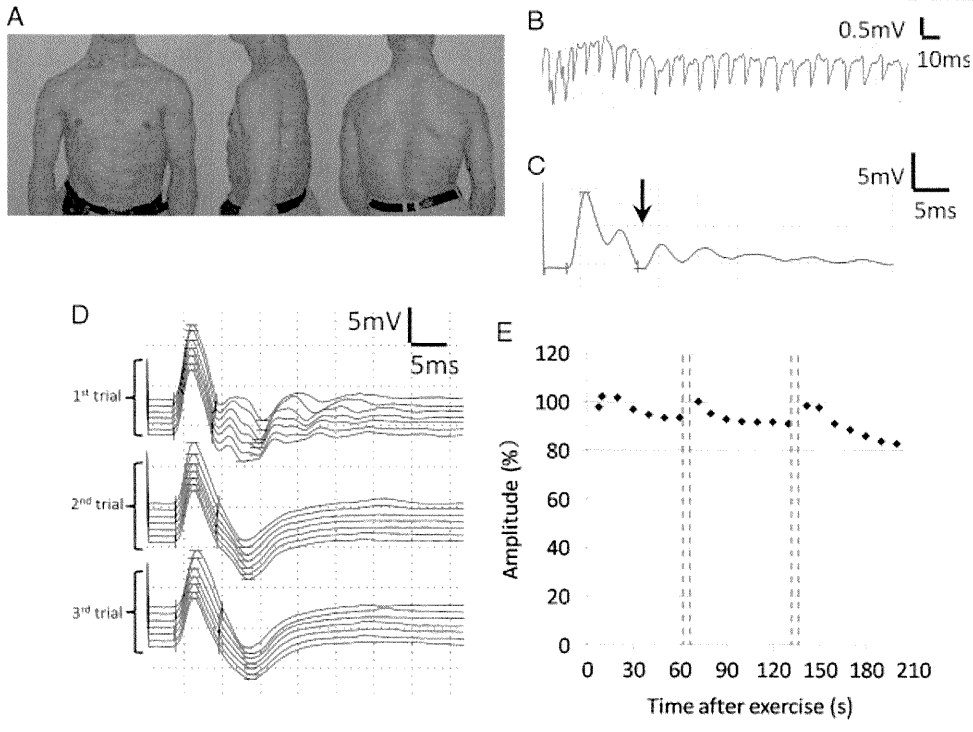

Figure 1. Clinical features of the patient. **A:** Images showing the hypertrophic upper body musculature of the patient. **B:** Needle electromyography recording of *tibialis anterior* muscle showed myotonic discharge. **C:** Compound muscle action potential (CMAP) recorded from *abductor digiti minimi* muscle showed postexercise myotonic potentials (PEMPs) (arrow). **D:** Traces of CMAP during the repeated short exercise test. PEMPs were observed in the first trial recording after 10-sec exercises, but disappeared with repeated exercises. **E:** A gradual decrease of the amplitude of CMAPs was observed with repeated short exercise.

Institutional Ethics Review Board at Osaka University. Genomic DNA was extracted from blood leukocytes from the patient and both parents. The regions encompassing all *SCN4A* (NM_000334.4) and *CLCN1* (NM_000083.2) exons were amplified by PCR (primer sequences and their location from the end of each exon are shown in Supp. Table S1), and the purified fragments were sequenced using an automated DNA sequencer (Big Dye Terminator v 3.1 and ABI310; PE Applied Biosystems, Foster City, CA). The PCR products including exon 21 and intron 21 were subcloned into the pCR2.1 TOPO vector (Invitrogen, Carlsbad, CA) and the nucleotide sequences of both alleles were determined. Nucleotide numbering reflects cDNA numbering with +1 corresponding to the A of the ATG translation initiation codon in the reference sequence, according to journal guidelines (www.hgvs.org/mutnomen). The translation initiation codon is codon 1.

mRNA Analysis

In addition to biopsied muscle from the patient, muscle specimens from myotonic dystrophy type 1 patients ($n = 3$) were used as disease controls. Total RNA was extracted from each sample using ISOGEN (Nippon Gene, Tokyo, Japan). First-strand cDNAs were synthesized from 1.8 μg of total RNA using random hexamers, and the cDNAs were amplified by 35 cycles of PCR (primer sequences in Supporting Information). The sizes of the PCR products were analyzed by agarose-gel electrophoresis stained with ethidium bromide, and the fluorescent intensity of each band was quantified using FluoroImager (GE Healthcare, Fairfield, CT). The RT-PCR products were cloned into the pCR2.1 TOPO vector, and the plasmids were transformed into competent *Escherichia coli* (ECOS^{TM} Competent E. Coli XL1-Blue, Nipongene, Tokyo, Japan). A total of 42 colonies were purified and sequenced.

Minigene Construction and Transient Transfection

The genomic fragment encompassing *SCN4A* exon 20 to exon 22 was amplified using the patient's genomic DNA (primer sequences in Supporting Information). Purified wild-type and mutant PCR fragments were cloned into the mammalian expression vector pcDNA3.1+ (Invitrogen). Clones were sequenced to exclude the presence of additional mutations.

U1 and U6 expression plasmids are described elsewhere [Roca and Krainer, 2009]. Mutations at the 5′ end of U1 or at the conserved U6 ACAGAG box were introduced by site-directed mutagenesis. All constructs were verified by sequencing.

HeLa cells were cultured in DMEM (Invitrogen) containing 10% (v/v) fetal bovine serum (FBS) and antibiotics (100 U ml^{-1} penicillin and 100 μg ml^{-1} streptomycin). We mixed 80 ng of the *SCN4A* minigenes with 400 or 800 ng of the U1 and U6 plasmids, and with 80 ng of the pEGFP-N1 plasmid (Clontech, Palo Alto, CA). HeLa cells were transfected with the plasmid mixes using FuGENE 6 (Roche Diagnostics, Indianapolis, IN) as previously reported [Roca and Krainer, 2009]. RNA was harvested 48 hr after transfection using TRIzol (Invitrogen). Residual DNA was eliminated with RQ1-DNase (Promega, Masdison, WI), and the RNA was recovered by phenol extraction and ethanol precipitation. A total of 1 μg of RNA was used for reverse transcription with Superscript II RT (Invitrogen) and oligo-dT as a primer.

The minigene cDNAs were amplified by PCR using primers located in the transcribed portion of the pcDNA3.1+ plasmid [Roca and Krainer, 2009]. The 5′ end of one of the PCR primers was radiolabeled using T4 polynucleotide kinase (New England Biolabs, Beverly, MA) and γ-^{32}P-ATP, and the primer was purified using MicroSpin G-25 columns (GE Healthcare). A total of 23 cycles of PCR were performed to ensure that amplification remained in the exponential phase. The PCR products were separated by 6% native PAGE, and the gels were exposed on BioMAX XAR film (Kodak, Rochester, NY). The identity of each band was determined by cloning of separate nonradioactive RT-PCR products into the Original TA Cloning kit (Invitrogen) followed by sequencing on an ABI3730 automated sequencer.

Construction of Expression Vector for the Aberrantly Spliced Isoform

Polymerase chain reaction (PCR) of the patient's cDNA was performed using primers shown in the Supporting Information. An Sse83871 (TaKaRa, Japan)-digested fragment of the PCR product was cloned into a mammalian expression construct for the human skeletal muscle sodium channel, pRc/CMV-hSkM1 [Takahashi and Cannon, 1999].

Na-Current Recording Using Cultured Cells

Cultures of human embryonic kidney (HEK) 293T cells and their transient transfection were performed as described [Green et al., 1998; Takahashi and Cannon, 1999]. In brief, plasmid cDNAs that encoded wild-type (0.8 μg/35-mm dish) or mutant human Na channel α-subunits (1.6 μg/35-mm dish), the human Na channel β-subunit (fourfold molar excess over α-subunit DNA), and a CD8 marker (0.1 μg/35-mm dish) were used to cotransfect HEK-293T cells by the calcium phosphate method. Transfection-positive cells are identified by attachment of CD8 antibody-coated beads (Dynal, Oslo Norway).

For measuring the current density, the same amount of α-subunit plasmids (1.6 μg/35-mm dish) were used for both wild-type and mutant channels. For the kinetic analyses, the amount of wild-type plasmid for transfection was reduced to one half of that of the mutant channel, because of the higher expression level of the wild-type channel.

At 2–3 days after transfection, we measured sodium currents using conventional whole-cell recording techniques with an Axopatch 200B amplifier (Molecular Devices, Sunnyvale, CA). Any cells with peak currents of <0.5 or >15 nA on step depolarization from −120 to −10 mV were discarded. The pipette (internal) solution consisted of: 105 mM CsF, 35 mM NaCl, 10 mM EGTA, and 10 mM Cs-HEPES (pH 7.4). The bath solution consisted of: 140 mM NaCl, 4 mM KCl, 2 mM $CaCl_2$, 1 mM $MgCl_2$, 5 mM glucose, and 10 mM Na-HEPES (pH 7.4).

The current density (pA/pF) was calculated using the capacitance of each cell and the peak current elicited by a depolarization pulse of −10 mV from a holding potential of −120 mV. The voltage dependence of steady-state fast inactivation was measured as the peak current elicited after a 300-msec conditioning pulse from a holding potential of −120 mV. The voltage dependence of steady-state slow inactivation was measured as the peak current elicited by the test pulse after a 60-sec conditioning prepulse, followed by a 20-msec gap at −120 mV to allow recovery from fast inactivation. The kinetics of the fast inactivation was characterized by measuring the voltage dependence of the time constant using three different protocols: (1) the current decay in the depolarized range; (2) the entry protocol in the

intermediate ranges; and (3) the recovery protocol in the hyperpolarized range.

Data Analysis

Curve fitting was manually performed off-line using Origin (Microcal LLC, Northampton, MA). Conductance was calculated as $G_{(V)} = I_{peak\,(V)}/(V - E_{rev})$, where the reversal potential, E_{rev}, was measured experimentally for each cell. The voltage dependence of activation was quantified by fitting the conductance measures to a Boltzmann function as $G_{(V)} = G_{max}/[1+\exp(-(V-V_{1/2})/k)]$. Steady-state fast inactivation was fitted to a Boltzmann function calculated as $I/I_{max} = 1/[1+\exp((V-V_{1/2})/k)]$, where $V_{1/2}$ was the half-maximum voltage and k was the slope factor. Steady-state slow inactivation was fitted to a Boltzmann function with the nonzero pedestal (S_0). Symbols with error bars indicate the mean± standard error of the mean (SEM). Statistical significance was determined using an unpaired t-test with Origin.

Simulation

Computer simulations of skeletal muscle were performed using the model previously reported by Cannon et al. [1993], with minor modifications. The model included potassium and sodium channels described with the Hodgkin-Huxley model and leak-current on the two electrically connected compartments (cell surface and the membrane of T-tubule system). We coded the model with Excel Visual Basic Application (Microsoft, Redmond, WA). Parameter values used for the wild type were identical with those reported previously [Hayward et al., 1996]. Parameters for fast inactivation of the mutant channel were estimated from the fit of experimental data with a two-state model.

Results

Clinical Electrophysiology and Muscle Histopathology

The patient was evaluated with clinical electrophysiological-methods. Myotonic discharges were present in all muscles examined by needle electromyography (Fig. 1B). The repeated short exercise test was performed to discriminate between myotonia caused by either Na or Cl channel mutations. After short exercises, abnormal sustained responses following the initial compound muscle action potential (CMAP) were observed, which were previously reported as postexercise myotonic potentials (PEMPs) (Fig. 1C) [Fournier et al., 2004, 2006]. During the repeated short exercise test, PEMPs disappeared (Fig. 1D) and the amplitude of CMAP decreased gradually (Fig. 1E). The observed postexercise decrease of electrical muscle response at room temperature was suggestive of myotonia caused by a Na-channel mutation.

Pathological examination of the biopsied muscle showed a myopathic change with marked variation in fiber size. Hypertrophic fibers with multiple internal nuclei were abundant. Type 1 fiber predominance and type 2B fiber deficiency were seen upon myosin ATPase staining (Supp. Fig. S1A–D). Acetylcholinesterase (AchE) activity was increased in the sarcolemma (Supp. Fig. S1E).

Analysis of Genomic DNA and mRNA Splicing Isoforms

Nucleotide sequence analysis of the patient's DNA showed no mutation in any exons of *SCN4A* and *CLCN1*. On electropherogram, however, two overlapping traces were consistently observed, starting from the sixth nucleotide downstream from the boundary between exon 21 and intron 21 of *SCN4A* (Supp. Fig. S2A). To analyze the sequences of each strand, the PCR products encompassing exon 21 and intron 21 were subcloned into the pCR2.1 TOPO vector. Sequence analysis of each strand revealed a heterozygous mutation in intron 21, which consists of a five-nucleotide deletion and one-nucleotide insertion at the sixth nucleotide downstream from the boundary between exon 21 and intron 21 (NG_011699.1:c.3912+6_3912+10delinsG) (Fig. 2A). Neither his parents nor 220 normal alleles harbored this mutation (Supp. Fig. S2A).

Because this mutation affects a portion of the 5′ splice site, we hypothesized that it might influence the splicing of intron 21. To examine the splicing patterns of the mutant transcript, RT-PCR was performed using mRNA extracted from skeletal muscle. In control muscles, only a fragment with the expected size (325 nucleotides) was observed. In muscle from the patient, however, two additional fragments were observed: one larger and the other smaller than normal. By measuring the fluorescent intensity of these bands, the proportion of each isoform was estimated as follows: large isoform: 33%; normal isoform: 57%; small isoform: 10% (Fig. 2B). To determine the nucleotide sequence, RT-PCR products were subcloned into the pCR2.1 TOPO vector. Sequence analysis showed that the smaller fragments consisted of two isoforms: one originated by splicing between a cryptic 5′ splice site in exon 21 and a cryptic 3′ splice site located at the initial portion of exon 22 (Deletion type: 2/42 colonies); the other one as a result of splicing from the 5′ splice site of exon 20 to the same cryptic 3′ splice site of exon 22 (Skip type: 8/42 colonies). Both small isoforms are predicted to be translated out of frame, with their reading frames interrupted by premature termination codons. The large isoform resulted from splicing between a cryptic 5′ splice site in intron 21 and the same cryptic 3′ splice site as above (retention type: 4/42 colonies). This isoform is in frame (Fig. 2C), and is predicted to encode a channel with a one-amino acid deletion and 35-amino acid insertion in the DIII-DIV linker of Nav1.4, which could retain some degree of functionality (Fig. 2D and Supp. Fig. S2B). It should also be noted that the AT-AC type II intron 21 was replaced with aberrant GT-AG introns in all the abnormal isoforms (Supp. Fig. S3).

Minigene Analysis Confirms the Molecular Diagnosis of the SCN4A Mutation

The deletion/insertion (TATCA>G) in intron 21 of one of the *SCN4A* alleles was a candidate mutation to cause the splicing defects associated with the patient's myotonia. This mutation affects position +6 (the sixth intronic nucleotide) of the 5′ splice site, which is one of the less conserved positions of GT-AG U2-type 5′ splice sites. In addition, the mutation also changes positions +7 and +8, which are not conserved at all in this class of 5′ splice sites. Nevertheless, these nucleotide changes at positions +6 to +8 reduce the base-pairing potential to the 5′ end of the U1 snRNA (Fig. 3A), which is an early essential interaction for 5′-splice-site selection in U2-type introns [Seraphin et al., 1988; Siliciano and Guthrie, 1988; Zhuang and Weiner, 1986]. In addition, the mutation also disrupts base-pairing to the conserved ACAGAG box in U6 snRNA (Fig. 3D), which replaces U1 later in spliceosome assembly [Kandels-Lewis and Seraphin, 1993; Lesser and Guthrie, 1993; Wassarman and Steitz, 1992]. In any case, because this is the first disease-associated 5′-splice-site mutation in an AT-AC type II intron,

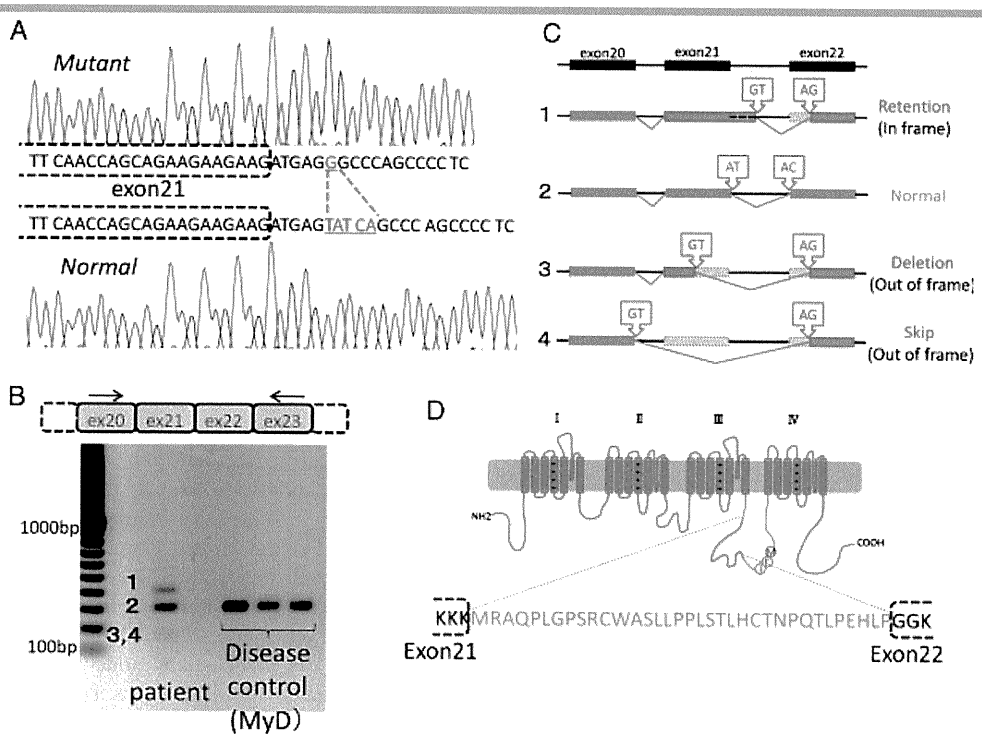

Figure 2. Genomic DNA and mRNA analysis. **A:** Both alleles of the patient's genomic DNA sequences around the boundary between exon 21 and intron 21 of *SCN4A* are separately shown. Deletion of five nucleotides (TATCA) and insertion of one nucleotide (*G*) were observed in one allele (c.3912+6_3912+10delinsG). **B:** RT-PCR from patient muscle mRNA revealed several aberrantly spliced isoforms, in addition to the normal isoform expressed in the disease control. Numbered bands (1–4) correspond to the isoforms in Figures 2C and 3C. Arrows indicate the primers used for RT-PCR. **C:** Summary of the sequence analysis of all isoforms. Lines indicate introns, and dark blue or red boxes indicate normal or aberrant exons, respectively. Light blue boxes indicate portions of the normal exons that were removed in the aberrant isoforms. Arrowhead rectangles indicate the splice-site dinucleotides. **D:** Schematic illustration of the mutant Nav 1.4 channel α subunit. The in-frame isoform encodes a large insertion (amino acids in blue type) in the domain III and IV linker.

additional evidence was necessary to unambiguously determine the pathogenicity of this mutation.

We transiently transfected HeLa cells with the wild-type and mutant *SCN4A* minigenes, and analyzed the splicing patterns by radioactive RT-PCR, as well as by cloning and sequencing to confirm the identity of the PCR products. Both *SCN4A* minigenes recapitulated the splicing patterns seen in either control or patient cells, respectively (Fig. 3B and C). The wild-type *SCN4A* minigene showed efficient splicing at the AT-AC type II boundaries, with traces of exon 21 skipping and activation of the cryptic GT-AG splice sites (Fig. 3C, lane 1). In contrast, the mutant minigene showed no splicing at the AT-AC splice sites, but gave rise to the same three aberrantly spliced isoforms seen in patient cells. These results confirmed the molecular diagnosis of the *SCN4A* intron 21 TATCA>G mutation as the cause of the patient's myotonia (Fig. 3C, lane 2).

The SCN4A Mutation Disrupts Base-Pairing to U1 and U6 snRNAs

We used genetic suppression analyses to investigate the molecular mechanisms underlying defective splicing due to the mutation at the AT-AC type II 5′ splice site in *SCN4A*. We cotransfected cells with the *SCN4A* mutant minigene with suppressor U1 and/or U6 snRNAs carrying compensatory mutations that restore base-pairing to the mutant 5′ splice site [Cohen et al., 1994; Mount and Anderson, 2000; Roca and Krainer, 2009; Seraphin et al., 1988; Siliciano and Guthrie, 1988; Zhuang and Weiner, 1986]. None of the multiple suppressor U1s carrying one or several compensatory mutations could rescue correct splicing at the AT-AC boundaries (Fig. 3C, lanes 3–8). In previous U1-suppressor experiments for U2-type GT-AG 5′ splice sites, restoring base-pairing to U1 snRNA alone was sufficient to rescue correct splicing [Roca and Krainer, 2009; Seraphin et al., 1988; Siliciano and Guthrie, 1988; Zhuang and Weiner, 1986], suggesting that the mutation at the *SCN4A* AT-AC type II 5′ splice site critically affects other recognition steps. The U6 suppressors alone could not rescue correct AT-AC splicing either (Fig. 3E, lane 3, and data not shown), in contrast to what was previously seen with mutant U2-type GT-AG 5′ splice sites [Carmel et al., 2004; Roca and Krainer, 2009]. Interestingly, combining certain suppressor U1 and U6 snRNAs rescued splicing via the AT-AC splice sites, albeit weakly (Fig. 3E, lane 6). This weak restoration of correct splicing could not be augmented by using different combinations of U1 and U6 suppressors, or by introducing additional compensatory mutations in U6 (Fig. 3E, lane 7, and data not shown). In some cases, a cryptic GT-AG splice-site pair was activated (Fig. 3C, lane 5, and Fig. 3E, lanes 6 and 7), for unknown reasons. Taken together, these results suggest that the *SCN4A* intron 21 TATCA>G mutation disrupts optimal base-pairing to both U1 and U6 snRNAs.

Current Density and Gating of the Mutant Channel

We examined the functional consequences of this aberrant splicing by recording whole-cell Na currents from HEK-293T cells transiently transfected with the mutant Na channel cDNA. The

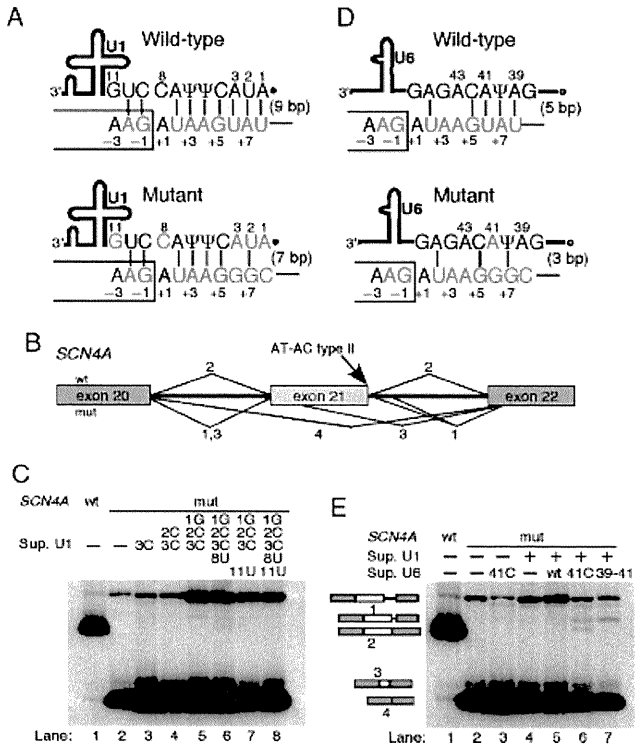

Figure 3. Mechanism of pathogenicity for the AT-AC type II intron mutation. **A:** Schematic of the base-pairing between the wild-type and mutant *SCN4A* intron 21 5′ splice site and the 5′ end of U1 snRNA. Thick line, U1 snRNA body; filled dot, trimethyl-guanosine cap; Ψ, pseudouridine. The box and the line depict portions of the exon and intron, respectively. Consensus and mutant nucleotides are shown in red and green, respectively. Nucleotides that were mutated in suppressor U1 snRNAs are shownin blue. The nucleotide positions at the 5′ splice site and at the 5′ end of U1 are numbered. Base pairs are depicted as vertical lines, and the total number is indicated in parenthesis. **B:** Schematic of the normal and aberrantly spliced isoforms shown in panel C. Isoforms are numbered as in Figure 2. The location of the AT-AC type II 5′ splice site is indicated. **C:** Suppressor U1 snRNAs alone could not rescue splicing at the mutant 5′ splice site. The *SCN4A* minigene and suppressor U1 used are indicated above the autoradiograms. The various mRNAs are indicated on the right, and correspond to those seen in patient cells (Fig. 2C). **D:** Schematic of the base pairing between the wild-type and mutant 5′ splice site and the conserved ACAGAG box of U6 snRNA. Open circle, γ-monomethyl cap. Font colors as in **A**. **E:** Suppressor U1 and U6 snRNAs partially rescue splicing at the mutant AT-AC type II 5′ splice site. The various constructs are indicated above the autoradiogram, and the identity of the mRNAs on the left. The U1 suppressor used was 1G2C3C, which together with the U6 suppressor 41C restored some correct splicing (lane 6).

current density of the mutant channel was approximately half that of the wild type (Fig. 4A).

Figure 4B shows normalized macroscopic Na currents of both wild-type and mutant channels, which were elicited by a depolarization pulse of −10 mV from a holding potential of −120 mV. The mutant channel current decayed more slowly than that of wild type, suggesting disruption of fast inactivation. The voltage dependence of steady-state fast inactivation measured with 300-msec conditioning pulse was shown in Figure 4A. The midpoint of the steady-state fast-inactivation curve for the mutant channel was shifted in the direction of depolarization by 19.1 mV compared to that of the wild type. The estimated parameters of steady-state fast inactivation were as follows: wild type: $V_{1/2} = -70.4 \pm 1.4$ ($n = 14$), $k = 5.0 \pm 0.2$ ($n = 14$); mutant: $V_{1/2} = -51.3 \pm 1.0$ ($n = 35$), $k = 7.0 \pm 0.2$ ($n = 35$) (Table 1). On the other hand, the voltage dependence of the mutant channel conductance was not different from that of the wild type (Fig. 4C and Table 1).

The voltage dependence of steady-state slow inactivation measured using a 60-sec conditioning prepulse was shown in Figure 4D. The midpoint of the steady-state slow inactivation curve for the mutant channel was shifted in the direction of depolarization by 8.1 mV compared to that of the wild type. The slope factor for the mutant channel was steeper than that of the wild type. However, the maximum extent of slow inactivation (S_0) did not differ between the wild-type and mutant channels (Table 1).

The kinetics of the fast inactivation was characterized by measuring the voltage dependence of the time constant using three different protocols. The time constants were analyzed by a single-exponential fit (see Supp. Fig. S4 for the analysis by two-exponential fit), in order to estimate the parameters of a two-state model, which are suitable for a simulation based on the Hodgkin-Huxley model. For the mutant channel, the voltage dependence of time constants was shifted in the direction of depolarization, and the time constants at the depolarized range were significantly slower (Supp. Fig. S5). Subsequently, the forward and backward rates of two-state model were estimated from the voltage dependence of steady-state fast inactivation and the time constants. For the mutant channel, the estimated value for the forward rate (α) was approximately four times and the backward rate (β) was one-fifth of those for wild type. The detail of the analysis is described in the Supporting Information.

Computer Simulation

Although the depolarized shift of steady-state fast-inactivation curve was consistent with enhanced membrane excitability, a computer simulation was performed to examine whether the functional defects of the mutant channel can recapitulate the symptoms, especially because the expression levels of the mutant channel could not be measured. The simulation based on the Hodgkin-Huxley model—which was previously reported by Cannon et al. [1993]—was reconstructed with Visual Basic. All the gating parameters for the wild-type channel were the same as those previously reported by Hayward et al. [1996] (Supp. Table S2). The parameters for fast inactivation of the mutant channel were modified based on the result in Supp. Figure S5. The fraction of the persistent current (f) for the mutant channel was estimated by averaging the currents in the last 5 msec of the 300-msec depolarization. All the other parameters for the mutant channel were identical to those for the wild type. The stimulating current was applied as a square wave (100 mA, 150 msec). Because the expression of the mutant channel is likely lower than that of the wild type, simulation studies were performed varying the proportion of the mutant channel. When the expressed Na channel was all wild type, repetitive firing of action potentials was not seen (data not shown). When the expression of the mutant channel was set at 50% of the total Na channel, repetitive firing of action potentials was observed (Fig. 5A). When the expression of the mutant channel was set at 35%, repetitive firing of action potentials was still evoked (Fig. 5B). Moreover, in the case of decreasing the expression of the mutant channel to 15%, repetitive firing of action potentials was still observed, although the degree of firing was not as robust (Fig. 5C). Overall, the results of this simulation suggest that the functional defect of the channel is sufficient to cause myotonia, even when the

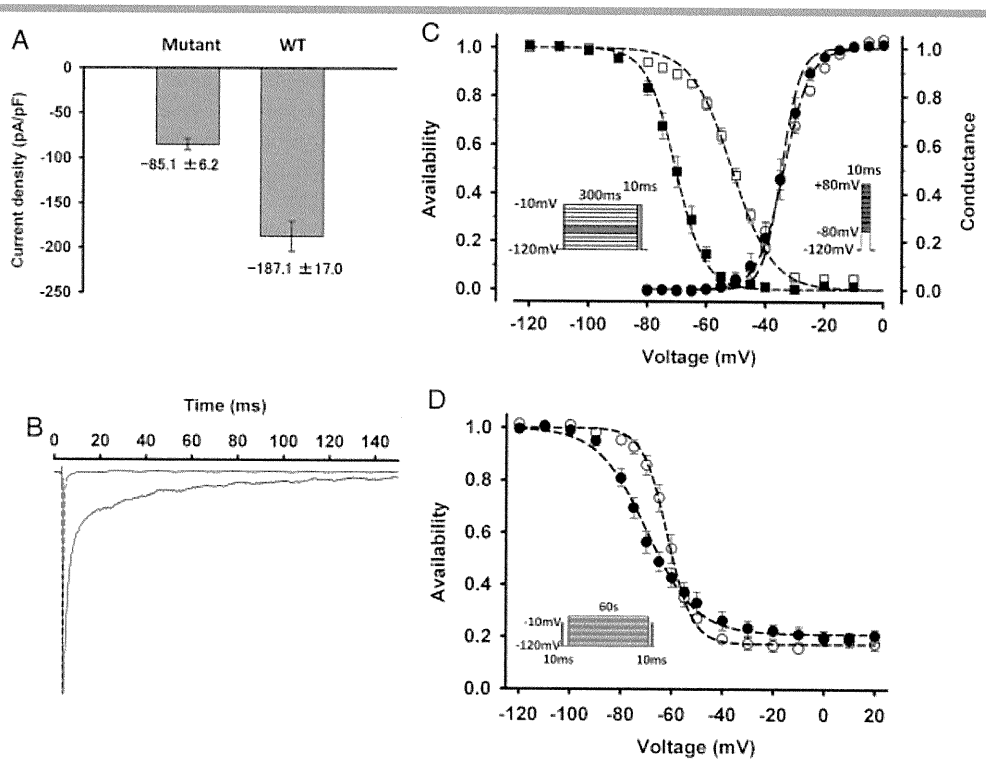

Figure 4. Current density and gating of the mutant channel. **A:** The current density (pA/pF) of the mutant channel ($n = 39$) is approximately half that of wild type ($n = 9$) when the same amount of the corresponding expression plasmids was used for transfection. Error bars indicate SEM. **B:** Normalized macroscopic sodium current elicited by a depolarization pulse of −10 mV from a holding potential of −120 mV. The mutant channel (solid line) showed slower decay than the wild type (dotted line), suggesting a disruption of fast inactivation. **C:** Voltage dependence of availability (steady-state fast inactivation, left, squares) and conductance (activation, right, circles). Filled and open symbols represent the wild-type and mutant channels, respectively. The midpoint of the steady-state fast inactivation curve for the mutant channel ($V_{1/2}$) was shifted in the direction of depolarization by 19.1 mV, compared to that for the wild type. The insets show the protocols used to measure the voltage dependence of steady-state fast inactivation (left) and the conductance (right). **D:** The voltage dependence of steady-state slow inactivation for the wild-type channel (filled symbols) and mutant channel (open symbols). The maximum extent of slow inactivation does not differ between the wild-type and mutant channels. The inset shows the protocol.

Table 1. Parameter Estimates for Wild-Type and Mutant Channels

	Activation		Fast inactivation		Slow inactivation		
	$V_{1/2}$ (mV)	k (mV/e-fold)	$V_{1/2}$ (mV)	k (mV/e-fold)	$V_{1/2}$ (mV)	k (mV/e-fold)	S_0
WT	−34.6±1.5 (14)	3.1±0.3* (14)	−70.4±1.4* (14)	5.0±0.2* (14)	−69.7±1.8* (9)	9.6±0.7* (9)	0.21±0.02 (9)
Mutant	−33.8±0.7 (35)	4.4±0.2* (35)	−51.3±1.0* (35)	7.0±0.2* (35)	−61.6±1.7* (7)	4.9±0.3* (7)	0.17±0.02 (7)

$V_{1/2}$ is the midpoint value of the steady-state inactivation curve and the voltage dependence of the conductance curve. k is the slope factor. S_0 is the nonzero pedestal. Values are means±SEM. *$P<0.01$.

expression of the mutant channel is as low as 15% of the total SCN4A channel.

Discussion

We have identified a causative mutation located in intron 21 of *SCN4A* in a patient with myotonia. The patient's myotonia was confirmed by needle electromyography, and was exacerbated by cold exposure and repetitive exercise (paramyotonia). Neurophysiological tests showed PEMPs and the characteristic decreasing of CMAPs with repeated short exercises [Fournier et al., 2004, 2006]. The clinical features and the results of the neurophysiological tests are consistent with myotonia due to a defect in Nav1.4. Hereditary skeletal–muscle diseases caused by mutations in *SCN4A* have been classified into paramyotonia congenita (PMC; MIM# 168300), potassium-aggravated myotonia (PAM; MIM# 608390), and hyperkalemic periodic paralysis (HyperPP; MIM# 170500) [Cannon, 2006]. Furthermore, the most severe form of PAM is called *myotonia permanens*, for which the only causative mutation reported to date is G1306E [Lehmann-Horn et al., 1990]. As the patient showed prominent generalized myotonia, associated with difficulty in breathing, hypertrophic musculature, joint contractures, and scoliosis, we assumed that his clinical features were indicative of *myotonia permanens*. Although he presented myotonia exacerbated by cold exposure, and paramyotonia in the eyelids, two symptoms characteristic of PMC rather than PAM, several cases of PAM exacerbated by cold exposure have been reported. As mentioned above, classification of sodium-channel myotonic disorders is sometimes difficult, because of their clinical overlap. Recently, the Consortium of Clinical Investigators of Neurological Channelopathies has proposed that sodium-channel myotonic disorders might be simply classified into two

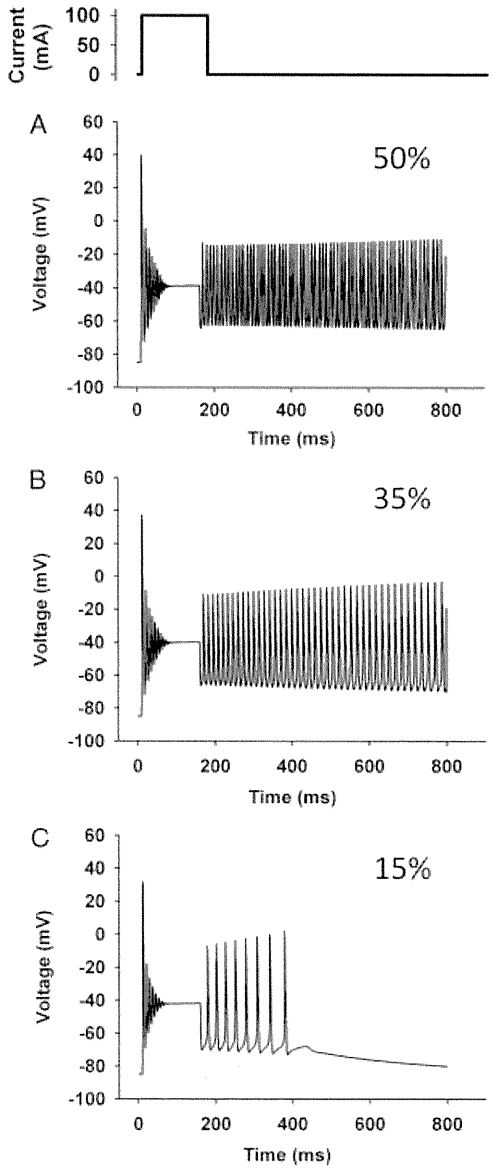

Figure 5. Computer simulation. The upper inset indicates the stimulating current (100 mA, 150 msec). The simulation was performed by varying the proportion of the mutant channel, because the expression of the mutant channel in the patient's muscle is unknown (**A:** 50%; **B:** 35%; **C:** 15%). Repetitive firing of action potentials was observed even when expression of the mutant channel was set at 15%.

broad groups, based on the presence or absence of episodic weakness: PMC or sodium-channel myotonia, respectively [Matthews et al., 2010]. According to this proposal, our case might be classified into sodium-channel myotonia, because of the lack of clear episodic weakness. Another clinical feature of interest is muscle atrophy in distal upper extremities. However, this would not exclude nondystrophic myotonia. In fact, dystrophic features have been reported in myotonia caused by Na-channel and Cl-channel mutations [Kubota et al., 2009; Nagamitsu et al., 2000; Plassart et al., 1996; Schoser et al., 2007].

From a clinicogenetic point of view, this mutation is unprecedented in two ways. First, this is the first disease-associated intronic mutation in a voltage-gated ion channel gene showing a gain-of-function defect. Many different mutations in voltage-gated ion channel genes have been identified as causes for inherited disorders, but these mutations mostly map to the coding exons [Cannon, 2006; George, 2005]. A few disease-associated mutations in noncoding regions of voltage-gated ion channel genes have been reported. For example, at least six mutations associated with autosomal-recessive (Becker) myotonia congenita have been identified in noncoding regions of the skeletal–muscle chloride-channel gene, *CLCN1* [Colding-Jorgensen, 2005]. Similarly, at least seven mutations causing Brugada syndrome have been identified in the noncoding regions of the cardiac muscle sodium-channel gene *SCN5A* [Ruan et al., 2009; Zimmer and Surber, 2008]. Notably, mutant channels causing Becker-type myotonia congenita and Brugada syndrome generally exhibit loss-of-function defects. Moreover, a splice-site mutation in the neuronal sodium channel *SCN1A* was identified in a patient with partial epilepsy with febrile seizures, although the properties of the mutant channel have not been assessed [Kumakura et al., 2009]. Here we described a heterozygous mutation in a non-coding region of *SCN4A* that causes aberrant splicing. Our results strongly suggest that one of the aberrantly spliced mRNA isoforms is translated into a functional channel that displays a gain-of-function defect. Therefore, our case constitutes a novel mechanism of pathogenesis for inherited channelopathies.

Second, the deletion/insertion in intron 21 of *SCN4A* is the first disease-associated mutation identified in a very rare class of introns, known as AT-AC type II. An intronic mutation in the other, more common type of AT-AC intron (AT-AC type I, or U12-dependent) in the *LKB1* gene was found to cause Peutz-Jeghers syndrome [Hastings et al., 2005]. No disease-associated mutation in AT-AC type II introns had been described until now, probably because of the very low number (only 15) of such introns in the human genome [Sheth et al., 2006]. Because 10 out of 15 AT-AC type II introns are found in members of Nav-channel gene family, other mutations in these introns may be found to be associated with channelopathies in the future.

The splicing defects caused by the *SCN4A* intron 21 mutation were confirmed by minigene analysis. The splicing patterns from the wild-type and mutant *SCN4A* minigenes faithfully matched those seen in control and patient cells, respectively. The disruption of the AT 5′ splice site resulted in aberrantly spliced mRNAs by activation of cryptic GT-AG pairs. This observation is consistent with the notion that AT 5′ splice sites are almost exclusively paired with AC 3′ splice sites [Dietrich et al., 1997; Parker and Siliciano, 1993; Sheth et al., 2006; Wu and Krainer, 1997].

Our genetic suppression experiments provided a mechanistic basis for the pathogenic effect of the deletion/insertion in intron 21. These tests suggested that the mutant AT-AC type II 5′ splice site is defective in efficient base-pairing to both U1 and U6 snRNAs, which are key splicing factors that sequentially bind U2-type 5′ splice sites. This might constitute a fundamental difference between AT-AC type II and GT-AG 5′ splice sites, in that 5′ splice-site mutations in GT-AG introns can usually be rescued by suppressor U1s alone [Roca and Krainer, 2009; Seraphin et al., 1988; Siliciano and Guthrie, 1988; Zhuang and Weiner, 1986], whereas in this case we only observed weak rescue when both U1 and U6 suppressors were expressed simultaneously. Further U1/U6 suppressor analysis using other AT-AC type II introns is needed to confirm the generality of the U6 dependence of *SCN4A* AT-AC type II introns.

Interestingly, the AT-AC type II mutation results in activation of cryptic U2-type GT-AG splice-site pairs, similarly to what was seen upon mutations in minor-spliceosome or U12-type introns [Hastings et al., 2005; Incorvaia and Padgett, 1998; Kolossova and Padgett, 1997]. These cryptic GT-AG pairs are present in the

wild-type pre-mRNA, but remain silent unless one of the AT-AC splice sites is mutated. Whereas GT-AG U2-type splice sites exhibit a very high degree of variation, with thousands of different sequences acting as functional splice sites in the human genome [Roca and Krainer, 2009], U12-type splicing elements (specifically the 5′ splice site and the branch point sequence) are very highly conserved, suggesting that these sequences are constrained to be functional [Sheth et al., 2006]. Our observations suggest that AT-AC type II introns are similarly constrained, and that one of these constraints might be the need for efficient base-pairing to U6 snRNA, possibly because of the G>A difference at the first intronic position. It remains possible that there are specific splicing elements and factors required for efficient splicing of AT-AC type II introns, but these are not identifiable by genomic analyses because of the very low number of such introns. In short, mutations that disrupt AT-AC type II splice sites, like those affecting U12-type splice sites, result in activation of cryptic U2-type GT-AG splice sites, because the sequence requirements for these U2-type GT-AG splice sites are much more flexible.

The functional properties of the aberrantly spliced channel provide further understanding about the molecular mechanism of fast inactivation of the sodium channel. It has been established that the DIII-DIV linker plays a key role in fast inactivation of sodium channels. In particular, a cluster of hydrophobic amino acids (IFM) in the DIII-DIV linker is believed to function as an essential component of the fast inactivation particle, which occludes the intracellular mouth of the activated channel by a " ball-and-chain" or "hinged-lid" mechanism [Armstrong and Bezanilla, 1977; West et al., 1992]. In Nav1.4, the DIII-DIV linker comprises 92 amino acids, but there are only 15 residues between the end of DIIIS6 and the IFM motif. To properly occlude the intracellular mouth of the channel, 10–20 residues between the end of DIIIS6 and the IFM motif are supposed to be optimal to form the hinged-lids structures [West et al., 1992]. The mutant sodium channel expressed in our patient's muscle has an insertion of 35 amino acids preceding the IFM motif, and showed disruption of fast inactivation. Considering the number of residues between the end of DIIIS6 and the IFM motif, the 35-amino acid insertion is probably too large and may give the "lid" more freedom of movement. Indeed, it has been reported that even a 12-amino-acid insertion into the 5′ end of the DIII-DIV linker (nine residues) and the beginning part of DIVS1 (three residues) causes disruption of fast inactivation [Patton and Goldin, 1991]. Therefore, it is highly possible that the elongated loop in our mutant channel does not properly function as the hinged lid, resulting in the disruption of fast inactivation.

The abnormally spliced channel expressed in cell culture showed disruption of fast inactivation, which is consistent with the hyperexcitability of the patient's skeletal muscle. In the case of heterozygous mutations located in coding regions (missense mutations), the proportion of the mutant channel might be expected to be half of the total channel, assuming equal expression. In the heterozygous patient described here, however, the expression of the aberrantly spliced mutant channel is likely less than half of the total channel. The proportion of mRNA coding for the abnormal channel was roughly estimated from the fluorometric measurement of the PCR fragments (Fig. 2B). The abundance of the mRNA for the mutant channel isoform was about 60% that of the normal isoform (Fig. 2B). The other mRNA isoforms were out of frame and introduced premature termination codons, so they are likely to be partially degraded by nonsense-mediated mRNA decay [Chang et al., 2007]. However, it is not certain whether the mutant channel is translated, correctly folded, and targeted to the plasma membrane as efficiently as the wild type. Indeed, the current density of mutant channel was about half that of wild type when expressed in HEK-293T cells, although this might also reflect a difference in the open probability between wild-type and mutant channels. Simply by multiplying the two numbers above, the expression ratio between the wild-type and mutant channels was estimated at 10:3. Computer simulation varying the expression level of the mutant showed that repetitive firing of action potentials (myotonia) is observed even if the expression of the mutant channel is set at 15% (Fig. 5). Taken together, the most likely explanation for our observations is that the functional defect of the mutant channel caused by aberrant splicing is sufficient to cause the patient's myotonic symptoms.

In summary, we have identified a rare nondystrophic myotonia caused by a mutation in the AT-AC type II intron in *SCN4A*. Our experiments also contribute to a better understanding of the splicing mechanisms for a very rare class of introns. Henceforth, the inherited channelopathies caused by mutations in noncoding regions should be investigated more vigorously.

Acknowledgments

The authors thank Dr. Steve Cannon for providing the expression vectors, Dr. Ryuzo Mizuno for referring the patient, and Ms. Mieko Tanaka for technical assistance.

References

Armstrong CM, Bezanilla F. 1977. Inactivation of the sodium channel. II. Gating current experiments. J Gen Physiol 70:567–590.

Brow DA. 2002. Allosteric cascade of spliceosome activation. Annu Rev Genet 36: 333–360.

Burge CB, Padgett RA, Sharp PA. 1998. Evolutionary fates and origins of U12-type introns. Mol Cell 2:773–785.

Cannon SC. 2006. Pathomechanisms in channelopathies of skeletal muscle and brain. Annu Rev Neurosci 29:387–415.

Cannon SC, Brown Jr RH, Corey DP. 1993. Theoretical reconstruction of myotonia and paralysis caused by incomplete inactivation of sodium channels. Biophys J 65:270–288.

Carmel I, Tal S, Vig I, Ast G. 2004. Comparative analysis detects dependencies among the 5′ splice-site positions. RNA 10:828–840.

Chang YF, Imam JS, Wilkinson MF. 2007. The nonsense-mediated decay RNA surveillance pathway. Annu Rev Biochem 76:51–74.

Cohen JB, Snow JE, Spencer SD, Levinson AD. 1994. Suppression of mammalian 5′ splice-site defects by U1 small nuclear RNAs from a distance. Proc Natl Acad Sci USA 91:10470–10474.

Colding-Jorgensen E. 2005. Phenotypic variability in myotonia congenita. Muscle Nerve 32:19–34.

Dietrich RC, Incorvaia R, Padgett RA. 1997. Terminal intron dinucleotide sequences do not distinguish between U2- and U12-dependent introns. Mol Cell 1:151–160.

Dutzler R, Campbell EB, Cadene M, Chait BT, MacKinnon R. 2002. X-ray structure of a ClC chloride channel at 3.0 A reveals the molecular basis of anion selectivity. Nature 415:287–294.

Fournier E, Arzel M, Sternberg D, Vicart S, Laforet P, Eymard B, Willer JC, Tabti N, Fontaine B. 2004. Electromyography guides toward subgroups of mutations in muscle channelopathies. Ann Neurol 56:650–661.

Fournier E, Viala K, Gervais H, Sternberg D, Arzel-Hezode M, Laforet P, Eymard B, Tabti N, Willer JC, Vial C, Fontaine B. 2006. Cold extends electromyography distinction between ion channel mutations causing myotonia. Ann Neurol 60:356–365.

George Jr AL. 2005. Inherited disorders of voltage-gated sodium channels. J Clin Invest 115:1990–1999.

Green DS, George Jr AL, Cannon SC. 1998. Human sodium channel gating defects caused by missense mutations in S6 segments associated with myotonia: S804F and V1293I. J Physiol 510(Pt 3):685–694.

Hastings ML, Resta N, Traum D, Stella A, Guanti G, Krainer AR. 2005. An LKB1 AT-AC intron mutation causes Peutz-Jeghers syndrome via splicing at noncanonical cryptic splice sites. Nat Struct Mol Biol 12:54–59.

Hayward LJ, Brown Jr RH, Cannon SC. 1996. Inactivation defects caused by myotonia-associated mutations in the sodium channel III-IV linker. J Gen Physiol 107:559–576.

Incorvaia R, Padgett RA. 1998. Base pairing with U6atac snRNA is required for 5′ splice site activation of U12-dependent introns in vivo. RNA 4:709–718.
Kandels-Lewis S, Seraphin B. 1993. Involvement of U6 snRNA in 5′ splice site selection. Science 262:2035–2039.
Kolossova I, Padgett R.A 1997. U11 snRNA interacts in vivo with the 5′ splice site of U12-dependent (AU-AC) pre-mRNA introns. RNA 3:227–233.
Kubota T, Kinoshita M, Sasaki R, Aoike F, Takahashi MP, Sakoda S, Hirose K. 2009. New mutation of the Na channel in the severe form of potassium-aggravated myotonia. Muscle Nerve 39:666–673.
Kumakura A, Ito M, Hata D, Oh N, Kurahashi H, Wang JW, Hirose S. 2009. Novel de novo splice-site mutation of SCN1A in a patient with partial epilepsy with febrile seizures plus. Brain Dev 31:179–182.
Lehmann-Horn F, Iaizzo PA, Franke C, Hatt H, Spaans F. 1990. Schwartz-Jampel syndrome: II. Na+ channel defect causes myotonia. Muscle Nerve 13:528–535.
Lesser CF, Guthrie C. 1993. Mutations in U6 snRNA that alter splice site specificity: implications for the active site. Science 262:1982–1988.
Matthews E, Fialho D, Tan SV, Venance SL, Cannon SC, Sternberg D, Fontaine B, Amato AA, Barohn RJ, Griggs RC, Hanna MG. 2010. The non-dystrophic myotonias: molecular pathogenesis, diagnosis and treatment. Brain 133:9–22.
Mount SM, Anderson P. 2000. Expanding the definition of informational suppression. Trends Genet 16:157.
Nagamitsu S, Matsuura T, Khajavi M, Armstrong R, Gooch C, Harati Y, Ashizawa T. 2000. A "dystrophic" variant of autosomal recessive myotonia congenita caused by novel mutations in the CLCN1 gene. Neurology 55:1697–1703.
Parker R, Siliciano PG. 1993. Evidence for an essential non-Watson-Crick interaction between the first and last nucleotides of a nuclear pre-mRNA intron. Nature 361:660–662.
Patel AA, Steitz JA. 2003. Splicing double: insights from the second spliceosome. Nat Rev Mol Cell Biol 4:960–970.
Patton DE, Goldin AL. 1991. A voltage-dependent gating transition induces use-dependent block by tetrodotoxin of rat IIA sodium channels expressed in *Xenopus* oocytes. Neuron 7:637–647.
Plassart E, Eymard B, Maurs L, Hauw JJ, Lyon-Caen O, Fardeau M, Fontaine B. 1996. Paramyotonia congenita: genotype to phenotype correlations in two families and report of a new mutation in the sodium channel gene. J Neurol Sci 142: 126–133.
Roca X, Krainer AR. 2009. Recognition of atypical 5′ splice sites by shifted base-pairing to U1 snRNA. Nat Struct Mol Biol 16:176–182.
Ruan Y, Liu N, Priori SG. 2009. Sodium channel mutations and arrhythmias. Nat Rev Cardiol 6:337–348.
Schoser BG, Schroder JM, Grimm T, Sternberg D, Kress W. 2007. A large German kindred with cold-aggravated myotonia and a heterozygous A1481D mutation in the SCN4A gene. Muscle Nerve 35:599–606.
Seraphin B, Kretzner L, Rosbash M. 1988. A U1 snRNA:pre-mRNA base pairing interaction is required early in yeast spliceosome assembly but does not uniquely define the 5′ cleavage site. EMBO J 7:2533–2538.
Sheth N, Roca X, Hastings ML, Roeder T, Krainer AR, Sachidanandam R. 2006. Comprehensive splice-site analysis using comparative genomics. Nucleic Acids Res 34:3955–3967.
Siliciano PG, Guthrie C. 1988. 5′ Splice site selection in yeast: genetic alterations in base-pairing with U1 reveal additional requirements. Genes Dev 2:1258–1267.
Takahashi MP, Cannon SC. 1999. Enhanced slow inactivation by V445M: a sodium channel mutation associated with myotonia. Biophys J 76:861–868.
Tsujino A, Maertens C, Ohno K, Shen XM, Fukuda T, Harper CM, Cannon SC, Engel AG. 2003. Myasthenic syndrome caused by mutation of the SCN4A sodium channel. Proc Natl Acad Sci USA 100:7377–7382.
Wassarman DA, Steitz JA. 1992. Interactions of small nuclear RNA's with precursor messenger RNA during in vitro splicing. Science 257:1918–1925.
West JW, Patton DE, Scheuer T, Wang Y, Goldin AL, Catterall WA. 1992. A cluster of hydrophobic amino acid residues required for fast Na(+)-channel inactivation. Proc Natl Acad Sci USA 89:10910–10914.
Wu Q, Krainer AR. 1996. U1-mediated exon definition interactions between AT-AC and GT-AG introns. Science 274:1005–1008.
Wu Q, Krainer AR. 1997. Splicing of a divergent subclass of AT-AC introns requires the major spliceosomal snRNAs. RNA 3:586–601.
Wu Q, Krainer AR. 1999. AT-AC pre-mRNA splicing mechanisms and conservation of minor introns in voltage-gated ion channel genes. Mol Cell Biol 19: 3225–3236.
Zhuang Y, Weiner AM. 1986. A compensatory base change in U1 snRNA suppresses a 5′ splice site mutation. Cell 46:827–835.
Zimmer T, Surber R. 2008. SCN5A channelopathies—an update on mutations and mechanisms. Prog Biophys Mol Biol 98:120–136.